Iterative strong coupling of dimensionally-heterogeneous models

Journal:	*International Journal for Numerical Methods in Engineering*
Manuscript ID:	draft
Wiley - Manuscript type:	Research Article
Date Submitted by the Author:	n/a
Complete List of Authors:	Leiva, Jorge; Instituto Balseiro Blanco, Pablo; Laboratório Nacional de Computação Científica, Ciência da Computação Buscaglia, Gustavo; Univ. Sao Paulo, ICMC
Keywords:	Complex systems, Coupled problems, Dimensionally-heterogeneous models, Strong coupling, Partitioned analysis

INTERNATIONAL JOURNAL FOR NUMERICAL METHODS IN ENGINEERING

Int. J. Numer. Meth. Engng 2000; **00**:1–6 *Prepared using* nmeauth.cls *[Version: 2002/09/18 v2.02]*

Iterative strong coupling of dimensionally–heterogeneous models

J. S. Leiva[1], P. J. Blanco[2] and G. C. Buscaglia[3,*]

[1] *Instituto Balseiro, Av. Bustillo Km. 9.5, San Carlos de Bariloche, 8400, Río Negro, Argentina, leivaj@ib.cnea.gov.ar*

[2] *Laboratório Nacional de Computação Científica, Av. Getúlio Vargas 333, Quitandinha, 25651–075, Petrópolis, RJ, Brazil, pjblanco@lncc.br*

[3] *Instituto de Ciências Matemáticas e Computação, Universidade de São Paulo, Av. do Trabalhador Sãocarlense 400, 13560-970 São Carlos, SP, Brazil, gustavo.buscaglia@icmc.usp.br*

SUMMARY

In this article we address decomposition strategies especially tailored to perform strong coupling of dimensionally-heterogeneous models, under the hypothesis that one wants to solve each submodel separately and implement the interaction between subdomains by boundary conditions alone. The novel methodology takes full advantage of the reduced number of interface unknowns in this kind of problems. Existing algorithms can be viewed as variants of the "natural" staggered algorithm in which each domain transfers function values to the other, and receives fluxes (or forces), and viceversa. This natural algorithm is known as Dirichlet-to-Neumann in the Domain Decomposition literature. Essentially, we propose a framework in which this algorithm is equivalent to applying Gauss–Seidel iterations to a suitably defined (linear or nonlinear) system of equations. It is then immediate to switch to other iterative solvers such as GMRES or other Krylov-based method, which we assess through

*Correspondence to: Instituto de Ciências Matemáticas e Computação, Universidade de São Paulo, Av. do Trabalhador Sãocarlense 400, 13560-970 São Carlos, SP, Brazil.

Received 15 December 2008

numerical experiments showing the significant gain that can be achieved. Indeed, the benefit is that an extremely flexible, automatic coupling strategy can be developed, which in addition leads to iterative procedures that are parameter-free and rapidly converging. Further, in linear problems they have the finite termination property.

KEY WORDS: Complex systems, Coupled problems, Dimensionally–heterogeneous models, Strong coupling, Partitioned analysis.

1. INTRODUCTION

Since the birth of computational mechanics, a massive amount of effort has been dedicated to the development of resolution schemes for solving a complex problem via the resolution of a series of simpler ones. As scientific computing has evolved towards the simulation of complex, multiscale multi–physics systems, the coupling of submodels of different dimensionality (and possible different physics) has become mandatory. Dimensionally–heterogeneous models are appropriate for situations in which several different geometrical scales play a role in the problem physics. A thorough motivation and discussion of partitioned analyses can be found in the article by Felippa et al. [1].

Realistic simulations of the circulatory system, for instance, only make sense if the regions of interest, that could be an aneurysm, a bifurcation, or the whole circle of Willis, are modeled with full 3D detailed models, while the rest of the major arteries is modeled with reduced one–dimensional equations, and the peripheral beds (arterioles, capillaries), and perhaps the heart, are approximated by lumped–parameter models [2, 3, 4, 5]. In this way, the simple models feed the detailed ones with appropriate information by means of coupling conditions, taking

into account the systemic interaction among the different components. Other examples can easily be found when modeling large heat conduction systems, as well as complex structures, both characterized by the presence of different geometrical scales. In this context, the use of dimensionally–heterogeneous models leads to a dramatic reduction in the computational costs while still providing insight on the detailed physics of the problem at the regions of interest [6, 7, 8, 9].

Nonetheless, solving the systems of equations arising from the coupling between submodels with different dimensions is a rather cumbersome task if performed in a monolithic fashion. In this article we address a procedure for developing decomposition strategies especially tailored for these systems, under the additional hypothesis that *one wants to solve each subdomain separately, and implement the interaction between domains just through the transfer of boundary information*. Classical approaches for this problem stem from classical domain decomposition techniques, such as the Dirichlet-to-Neumann method. Nonetheless, their flexibility with respect to the choice of boundary conditions in the subdomains is rather limited, and also they lead to Richardson–like iterative relaxation methods which require parameter tuning to ensure convergence. Other approaches available in the literature, are the procedures presented in [10] in the context of fluid-structure interaction problems. Also, in [11] the authors solve a series of problems to approximate the solution to the Navier–Stokes equations when imposing flow rate boundary conditions, whereas in [12] the same problem is addressed by using a Schur complement scheme.

Due to the application we are aiming at, we propose an alternative methodology that takes full advantage of the reduced number of interface unknowns when coupling dimensionally–heterogeneous models. Though the procedure is general, we describe it for steady heat

conduction problems. In addition to the (mean) temperature at each interface we add the heat flux as interface variable. When the number of interfaces is N, this leads to $2N$ unknown interface variables. If N is small this poses no difficulty, and the benefit is that an extremely flexible, automatic coupling strategy can be developed, which, in addition, leads to an iterative procedure with the finite termination property for linear problems, because it converges in $2N$ iterations.

It should be noted that we address here the solution of the system of equations arising from a partitioned system, which we assume has a unique solution. The partitioning itself has been discussed by other authors (see the article by Park and Felippa [13] and references therein). In relation to the available literature, the strategy we propose can be viewed as a new procedure of *strong coupling* [14] which is specially attractive in the context of dimensionally–heterogeneous partitioned systems.

The present work is organized as follows: Section 2 begins with some quite simple examples in order to present the ideas. Section 3 extends the concept of the previous section for dimensionally–heterogeneous models, while Section 4 provides examples of application to show the potentialities of the methodology. In Section 5 some additional remarks are presented. Finally, in Section 6 the conclusions are drawn.

2. PARTITIONING OF SIMPLE COUPLED PROBLEMS

In this section some basic illustrative examples are discussed that aim at revealing the proposed coupling strategy.

2.1. 1D–1D partitioning of a coupled problem

Consider the diffusion problem defined in the 1D domain of length L shown in Figure 1; i.e.,

$$\begin{cases} -\dfrac{d}{dx}\left(k\dfrac{dU}{dx}\right) = f \quad \text{in } (0,L), \\ U(0) = 0, \\ U(L) = 0. \end{cases} \tag{1}$$

To keep the exposition as simple as possible, let us assume that k and f are constants, and

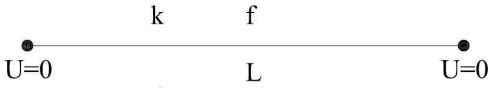

Figure 1. Diffusion problem in a 1D domain.

that homogeneous Dirichlet boundary conditions are applied at the boundaries.

We decompose the domain into two non-overlapping regions $\Omega_1 = (0,c)$, $\Omega_2 = (c,L)$. Our aim, as in all domain decomposition methods, is to solve problem (1) by solving separate problems in Ω_1 and Ω_2. For the partitioned solution (U_1, U_2) to coincide with the exact one, in the sense that $U_1 = U_{|\Omega_1}$ and $U_2 = U_{|\Omega_2}$, it is necessary and sufficient that both functions, together with their fluxes, match at point c. In other words, defining the (unknown) *coupling variables* u_c and q_c, the following must hold

$$\begin{aligned} U_1(c) = U_2(c) = u_c, \\ -k\frac{dU_1}{dx}(c) = -k\frac{dU_2}{dx}(c) = q_c. \end{aligned} \tag{2}$$

We focus first on Ω_1, in which we will solve the original equation $(1)_1$ with boundary condition $(1)_2$, but we are missing a boundary condition at $x = c$. Let us decide, arbitrarily, that $x = c$

will be a *Dirichlet* boundary for Ω_1. If we impose a value γ, the solution w_γ of

$$\begin{cases} -\dfrac{d}{dx}\left(k\dfrac{dw_\gamma}{dx}\right) = f \quad \text{in } (0,c), \\ w_\gamma(0) = 0, \\ w_\gamma(a) = \gamma, \end{cases} \tag{3}$$

will depend on γ, as implied by the subscript. Let us denote by $\mathcal{Q}_c^1(\gamma)$ the flux at $x = c$ corresponding to the solution w_γ, i.e.,

$$\mathcal{Q}_c^1(\gamma) = -k\frac{dw_\gamma}{dx}(c). \tag{4}$$

It is then clear that, for (q_c, u_c) to satisfy (2), they must satisfy the equation

$$-q_c + \mathcal{Q}_c^1(u_c) = 0. \tag{5}$$

Let us turn now to Ω_2, and arbitrarily decide that we want $x = c$ to be a *Neumann* boundary for it. Proceeding analogously as above, let z_δ be the solution of

$$\begin{cases} -\dfrac{d}{dx}\left(k\dfrac{dz_\delta}{dx}\right) = f \quad \text{in } (c,L), \\ z_\delta(L) = 0, \\ -k\dfrac{dz_\delta}{dx}(c) = \delta, \end{cases} \tag{6}$$

and let us denote by $\mathcal{U}_c^2(\delta)$ the value of z_δ at $x = c$, i.e.,

$$\mathcal{U}_c^2(\delta) = z_\delta(c). \tag{7}$$

With this notation, it is clear that (q_c, u_c) must satisfy

$$-\mathcal{U}_c^2(q_c) + u_c = 0. \tag{8}$$

Remark 1. *In our simple example $\mathcal{Q}_c^1$ and $\mathcal{U}_c^2$ can be calculated explicitly. They are given by*

the affine functions

$$\mathcal{Q}_c^1(\gamma) = -\frac{k}{c}\gamma + \frac{cf}{2}, \tag{9}$$

$$\mathcal{U}_c^2(\delta) = \frac{L-c}{k}\delta + \frac{f\,(L-c)^2}{2k}. \tag{10}$$

We thus arrive at a system of two equations in the two unknowns q_c and u_c

$$\begin{aligned} r_1(q_c, u_c) &:= -q_c + \mathcal{Q}_c^1(u_c) = 0, \\ r_2(q_c, u_c) &:= -\mathcal{U}_c^2(q_c) + u_c = 0. \end{aligned} \tag{11}$$

We group the unknowns into the vector $X = (q_c, u_c)$ and the residuals into the vector $r(X) = (r_1(X), r_2(X))$. Whether these are row or column vectors will be obvious from the context.

Up to now we have made two arbitrary choices, namely to take $x = c$ as Dirichlet bondary for Ω_1 and as Neumann boundary for Ω_2. Let us make a third arbitrary choice and solve the system above by the *Gauss-Seidel* method starting from $X_0 = (q_c^0, u_c^0)$. This leads to the iterative method

$$\begin{aligned} q_c^{k+1} &= \mathcal{Q}_c^1(u_c^k), \\ u_c^{k+1} &= \mathcal{U}_c^2(q_c^{k+1}), \end{aligned} \tag{12}$$

which is nothing but the classical *Dirichlet-to-Neumann* (D-to-N) method of domain decomposition.

Notice that, in the simple case in which k and f are constants, eliminating q_c^{k+1} from the previous equations leads to

$$u_c^{k+1} = -\frac{L-c}{c}u_c^k + \frac{fL(L-c)}{2k}, \tag{13}$$

implying that

$$u_c^{k+1} - u_c = -\frac{L-c}{c}(u_c^k - u_c),$$

so that if $c > L/2$ the method will converge linearly, with constant $(L-c)/c$, and if $c \leq L/2$ it will not converge. Taking, for example, $L = 3$, $c = f = k = 1$, $q_c^0 = u_c^0 = 0$, leads to $q_c^1 = 1/2$, $u_c^1 = 3$, $q_c^2 = -5/2$, $u_c^2 = -3$, etc., diverging from the exact solution $q_c = -1/2$, $u_c = 1$.

The reinterpretation of the D-to-N method introduced above allows us to study many alternatives simply by changing the choices made along the derivation. Let us work out some of these alternatives in detail.

Consider for example changing the Gauss-Seidel solution of (11) by the following matrix–free GMRES technique:

1. Given X_0, compute $r(X_0)$, set $Z = \|r(X_0)\|_2$, and $v_1 = r(X_0)/Z$.
2. For $j = 1, \ldots, m$, do
3. Compute $w_j = r(X_0) - r(X_0 + v_j)$
4. For $i = 1, \ldots, j$, do
5. $H_{ij} = (w_j, v_i)$
6. $w_j = w_j - H_{ij} v_i$
7. Enddo
8. $H_{j+1,j} = \|w_j\|_2$. If $H_{j+1,j} = 0$ set $m = j$ and goto 11
9. $v_{j+1} = w_j / H_{j+1,j}$
10. Enddo
11. Define the $(m+1) \times m$ Hessenberg matrix $\mathsf{H}_m = \{H_{ij}\}_{1 \leq i \leq m+1, 1 \leq j \leq m}$

12. Compute y_m, the minimizer of $\|Ze_1 - \mathsf{H}_m y\|_2$

13. Do $X_m = X_0 + \mathsf{V}_m y_m$, where the columns of V_m are the vectors v_j computed through the iterations.

With the same data as before, and in particular $X_0 = (q_c^0, u_c^0) = (0, 0)$, one obtains

$$r(X_0) = \begin{pmatrix} \frac{1}{2} \\ -2 \end{pmatrix}, \qquad v_1 = \frac{1}{\sqrt{17}} \begin{pmatrix} 1 \\ -4 \end{pmatrix},$$

to calculate $r(X_0)$ we solved on Ω_1 with Dirichlet boundary condition equal to u_c^0 and on Ω_2 with Neumann boundary condition equal to q_c^0. We now need to calculate $r(X_0 + v_1)$. For this purpose we solve on Ω_1 with Dirichlet condition equal to $(X_0 + v_1)_2 = -\frac{4}{\sqrt{17}}$ and on Ω_2 with Neumann condition equal to $(X_0 + v_1)_1 = \frac{1}{\sqrt{17}}$, this leads to

$$w_1 = r(X_0) - r(X_0 + v_1) = \frac{1}{\sqrt{17}} \begin{pmatrix} -3 \\ 6 \end{pmatrix}, \qquad H_{11} = (w_1, v_1) = -\frac{27}{17},$$

$$w_1 = w_1 - H_{11} v_1 = -\frac{6}{17^{\frac{3}{2}}} \begin{pmatrix} 4 \\ 1 \end{pmatrix}, \qquad H_{21} = \frac{6}{17},$$

$$v_2 = -\frac{1}{\sqrt{17}} \begin{pmatrix} 4 \\ 1 \end{pmatrix}.$$

We now calculate $r(X_0 + v_2)$ imposing $(X_0 + v_2)_2$ as Dirichlet condition for Ω_1 and $(X_0 + v_2)_1$ as Neumann condition for Ω_2. Notice that the GMRES algorithm does not impose to the Neumann domain the flux obtained from the Dirichlet domain or viceversa. The consequence is that, once the orthogonalization steps 4–7 are completed, we end up with $w_2 = 0$ (which was expected, since the space is two-dimensional). As a result, step 12 yields

$$\begin{pmatrix} -\frac{27}{17} & \frac{23}{17} \\ \frac{6}{17} & \frac{27}{17} \end{pmatrix} \begin{pmatrix} y_1 \\ y_2 \end{pmatrix} = \begin{pmatrix} \frac{\sqrt{17}}{2} \\ 0 \end{pmatrix} \quad \Rightarrow \quad y = \frac{1}{2\sqrt{17}} \begin{pmatrix} -9 \\ 2 \end{pmatrix},$$

leading to

$$X_2 = X_0 + y_1 v_1 + y_2 v_2 = \begin{pmatrix} -\frac{1}{2} \\ 1 \end{pmatrix} = \begin{pmatrix} q_c \\ u_c \end{pmatrix},$$

the exact result.

The point we have made in the simple exercise above is that, keeping the same choices of boundary conditions as in the D-to-N method (Dirichlet for Ω_1, Neumann for Ω_2), by changing the solver to GMRES we obtain convergence in two iterations for any choice of parameters and of initial guess.

Let us now keep the GMRES solver and change the boundary condition to Dirichlet for both subdomains. The system now becomes

$$\begin{aligned} r_1(q_c, u_c) &:= -q_c + \mathcal{Q}_c^1(u_c) = 0, \\ r_2(q_c, u_c) &:= -q_c + \mathcal{Q}_c^2(u_c) = 0, \end{aligned} \tag{14}$$

where $\mathcal{Q}_c^2(u_c)$ is the flux obtained at $x = c$ when the equation is solved in Ω_2 with Dirichlet condition (at $x = c$) with value u_c. In this very simple case we have

$$\mathcal{Q}_c^2(\gamma) = \frac{k}{L-c}\gamma - \frac{f(L-c)}{2}. \tag{15}$$

Taking the same values as before, we get

$$r(X_0) = \begin{pmatrix} \frac{1}{2} \\ -1 \end{pmatrix}, \qquad v_1 = \frac{1}{\sqrt{5}} \begin{pmatrix} 1 \\ -2 \end{pmatrix}.$$

To evaluate $r(X_0+v_1)$ we now solve the equation on both domains with the Dirichlet conditions given by $(X_0 + v_1)_1 = \frac{1}{\sqrt{5}}$ and $(X_0 + v_1)_2 = -\frac{2}{\sqrt{5}}$ for Ω_1 and Ω_2 respectively, which gives

$$r(X_0 + v_1) = \begin{pmatrix} \frac{1}{\sqrt{5}} + \frac{1}{2} \\ -\frac{2}{\sqrt{5}} - 1 \end{pmatrix}.$$

This leads to $H_{11} = -1$ and $H_{21} = 0$, and the process ends after a single iteration. The result is obtained from

$$H_{11}y_1 = Z \quad \Rightarrow \quad y_1 = -Z = -\frac{\sqrt{5}}{2} \quad \Rightarrow \quad X_1 = X_0 + y_1 v_1 = \begin{pmatrix} -\frac{1}{2} \\ \\ 1 \end{pmatrix},$$

which is again exact. Notice that the convergence in just one iteration does not always take place. If the initial condition is modified to $q_c^0 = u_c^0 = 1$, for example, two iterations are needed.

2.2. Multiple 1D partitions

Let us now consider a partition of $\Omega = (0, L)$ consisting of $N+1$ subdomains, Ω_1, $\Omega_2, \ldots, \Omega_{N+1}$, with an interface given by the set Σ consisting of N points c_1, $c_2, \ldots, c_N$. The ideas above are easily extended to such a partition. To see this, let us summarize them as a strategy consisting of four steps:

Step 1 *Define two interface variables at each point of* Σ, representing the variables on which continuity is to be enforced (q and u, in the examples). For an interface consisting of N points, these variables will be denoted by $q_1, u_1, q_2, u_2, \ldots, q_N, u_N$.

Step 2 *Choose a type of boundary condition at each point of* Σ *for each of the two subdomains that have it as boundary.* The chosen type of boundary conditions for each Ω_i must lead to a well-posed problem in it, but is otherwise arbitrary. Choosing Dirichlet or Neumann conditions on one side of Σ, for example, does not depend on the choice made on the other side of Σ. Coloring of subdomains is thus unnecessary. For simplicity, we restrict for the time being to either Dirichlet or Neumann types, but Robin conditions are perfectly possible, as will be discussed later on.

Step 3 *Set up a system of equations for the interface variables* (the q_i's and u_i's). Each of the two subdomains sharing any given point c_i of Σ contributes one equation which only involves calculations internal to the subdomain. The corresponding equation depends on whether c_i is taken as Dirichlet or Neumann boundary.

Step 4 *Iteratively solve the corresponding system to find the interface variables.* Not any iterative method is possible, because some of the coefficients of the system of equations are not explicitly available. Any jacobian-free method, however, should be easily applicable.

The practical interest of the previous strategy can now be discussed. In (*Step 1*) a set of $2N$ interface variables, $q_1, u_1, \ldots, q_N, u_N$ is defined. Then we choose a boundary condition at each interface for each subdomain. Here we point out that the solution (w_i) in subdomain (c_{i-1}, c_i) is not defined if Neumann conditions are imposed over both endpoints. We take, for example, the left endpoint as Dirichlet boundary and the right one as Neumann boundary. The two equations provided by subdomain i (excluding the leftmost, $i = 1$, and rightmost, $i = N + 1$, subdomains, which receive special treatment) are:

$$-q_{i-1} + \mathcal{Q}_i^L(u_{i-1}, q_i) = 0, \tag{16}$$

$$-\mathcal{U}_i^R(u_{i-1}, q_i) + u_i = 0, \tag{17}$$

where the operators $\mathcal{Q}_i^L$ and $\mathcal{U}_i^R$ are defined as follows:

$$\mathcal{Q}_i^L(u_{i-1}, q_i) = -k_i(c_{i-1})\frac{dw_i}{dx}(c_{i-1}), \tag{18}$$

$$\mathcal{U}_i^R(u_{i-1}, q_i) = w_i(c_i), \tag{19}$$

with w_i the solution of the local problem

$$\begin{cases} -\dfrac{d}{dx}\left(k_i \dfrac{dw_i}{dx}\right) = f_i \quad \text{in } (c_{i-1}, c_i), \\ w_i(c_{i-1}) = u_{i-1}, \\ -k_i(c_i)\dfrac{dw_i}{dx}(c_i) = q_i. \end{cases} \tag{20}$$

These $2(N-1)$ equations are supplemented with one equation coming from the leftmost subdomain, which is either $q_1 - \mathcal{Q}_1^R(u_1) = 0$ or $-\mathcal{U}_1^R(q_1) + u_1 = 0$ depending on the boundary condition chosen, and the other equation coming from the rightmost subdomain (again depending on the chosen boundary condition). The resulting $2N$ equations can then be solved iteratively with any jacobian-free iterative algorithm for linear systems. The analysis of the convergence of any specific algorithm is outside the scope of this paper, but it is obvious that any Krylov–subspace method will converge in at most $2N$ iterations.

To render the ideas more evident, let us consider in Figure 1 the following three-subdomain partition ($N = 2$) $\Omega_1 = (0, c_1)$, $\Omega_2 = (c_1, c_2)$ and $\Omega_3 = (c_2, L)$. In this case the unknown vector would be $X = (q_1, u_1, q_2, u_2)$ and the system of equations would read

$$\begin{aligned} r_1(q_1, u_1) &:= -q_1 + \mathcal{Q}_1^R(u_1) = 0, \\ r_2(q_1, u_1, q_2) &:= -q_1 + \mathcal{Q}_2^L(u_1, q_2) = 0, \\ r_3(u_1, q_2, u_2) &:= -\mathcal{U}_2^R(u_1, q_2) + u_2 = 0, \\ r_4(q_2, u_2) &:= -\mathcal{U}_3^L(q_2) + u_2 = 0. \end{aligned} \tag{21}$$

Schematically, this corresponds to the linear system (which is of course never built explicitly)

$$\begin{pmatrix} -1 & C_{11}^R & 0 & 0 \\ -1 & C_{11}^L & D_{12}^L & 0 \\ 0 & E_{21}^R & F_{22}^R & 1 \\ 0 & 0 & F_{22}^L & 1 \end{pmatrix} \begin{pmatrix} q_1 \\ u_1 \\ q_2 \\ u_2 \end{pmatrix} = \begin{pmatrix} b_1^R \\ b_2^L \\ b_2^R \\ b_3^L \end{pmatrix}. \tag{22}$$

Notice from the first and last equations in (21) or (22) that we have adopted c_1 as Dirichlet boundary for Ω_1 and c_2 as Neumann boundary for Ω_3. Along the iterative process, which will converge in at most four iterations, one solves one problem in each subdomain per iteration. In Ω_2, for example, at each iteration one solves the differential equation with Dirichlet condition on the left equal to the current value of u_1 and Neumann condition on the right equal to the current value of q_2, as implicitly stated in (21). These conditions differ from the function value and flux yielded by the neighboring elements, which in our notation would be $\mathcal{U}_1^R(q_1)$ and $\mathcal{Q}_3^L(u_2)$. There is thus no "direct transfer" of boundary conditions. The sequence of boundary conditions along the iterations is provided by the iterative algorithm itself.

It is quite easy to find a situation in which the traditional D-to-N procedure fails to converge for this three-subdomain partition. On the other hand, the resolution of the interface coupling problem, again through the GMRES algorithm, takes four iterations to attain the exact solution.

2.3. Remark on 2D domain decomposition

The same ideas can be applied for the domain decomposition of a 2D problem. To do that, consider a heat conduction problem in the setting shown in Figure 2(a), with coupling interface Γ_c, and Dirichlet boundary conditions applied over Γ_D. Further, consider a mesh–based discretization method, such as the finite element method, in each subdomain. In Figure 2(b) the *matching* meshes for the two subdomains are shown.

The coupling variables defined over the coupling interface Γ_c are now the temperature u_x and normal heat flux q_x with $x = a, b, c, d, e, f$ (in the discrete formulation of the problems in Ω_1 and Ω_2 these quantities are precisely defined). We can now choose the type of boundary

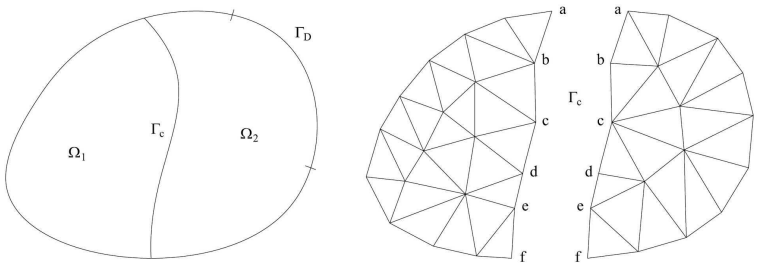

(a) Partitioning of the domain. (b) Meshes for both partitions.

Figure 2. Diffusion problem in a 2D domain.

conditions arbitrarily. Let a, b and c be Dirichlet nodes for Ω_1, and d, e and f be Neumann nodes. On the other hand, let a, c and e be Dirichlet nodes for Ω_2, while b, d and f are Neumann nodes. The system of equations is thus given by (with notation analogous to that

of the 1D examples):

$$
\begin{aligned}
&-q_a + \mathcal{Q}_a^1(u_a, u_b, u_c, q_d, q_e, q_f) = 0 \\
&-q_a + \mathcal{Q}_a^2(u_a, q_b, u_c, q_d, u_e, q_f) = 0 \\
&-q_b + \mathcal{Q}_b^1(u_a, u_b, u_c, q_d, q_e, q_f) = 0 \\
&-\mathcal{U}_b^2(u_a, q_b, u_c, q_d, u_e, q_f) + u_b = 0 \\
&-q_c + \mathcal{Q}_c^1(u_a, u_b, u_c, q_d, q_e, q_f) = 0 \\
&-q_c + \mathcal{Q}_c^2(u_a, q_b, u_c, q_d, u_e, q_f) = 0 \\
&-\mathcal{U}_d^1(u_a, u_b, u_c, q_d, q_e, q_f) + u_d = 0 \\
&-\mathcal{U}_d^2(u_a, q_b, u_c, q_d, u_e, q_f) + u_d = 0 \\
&-\mathcal{U}_e^1(u_a, u_b, u_c, q_d, q_e, q_f) + u_e = 0 \\
&-q_e + \mathcal{Q}_e^2(u_a, q_b, u_c, q_d, u_e, q_f) = 0 \\
&-\mathcal{U}_f^1(u_a, u_b, u_c, q_d, q_e, q_f) + u_f = 0 \\
&-\mathcal{U}_f^2(u_a, q_b, u_c, q_d, u_e, q_f) + u_f = 0
\end{aligned}
\tag{23}
$$

where the first, third, fifth, seventh, nineth and eleventh equations arise from the first subdomain, and the others from the second one.

Since the problem within each subdomain is linear, these equations are implicitly

representing a linear system of the form

$$\begin{pmatrix}
-1 & C^1_{aa} & 0 & C^1_{ab} & 0 & C^1_{ac} & D^1_{ad} & 0 & D^1_{ae} & 0 & D^1_{af} & 0 \\
-1 & C^2_{aa} & D^2_{ab} & 0 & 0 & C^2_{ac} & D^2_{ad} & 0 & 0 & C^2_{ae} & D^2_{af} & 0 \\
0 & C^1_{ba} & -1 & C^1_{bb} & 0 & C^1_{bc} & D^1_{bd} & 0 & D^1_{be} & 0 & D^1_{bf} & 0 \\
0 & -E^2_{ba} & -F^2_{bb} & 1 & 0 & -E^2_{bc} & -F^2_{bd} & 0 & 0 & -E^2_{be} & -F^2_{bf} & 0 \\
0 & C^1_{ca} & 0 & C^1_{cb} & -1 & C^1_{cc} & D^1_{cd} & 0 & D^1_{ce} & 0 & D^1_{cf} & 0 \\
0 & C^2_{ca} & D^2_{cb} & 0 & -1 & C^2_{cc} & D^2_{cd} & 0 & 0 & C^2_{ce} & D^2_{cf} & 0 \\
0 & -E^1_{da} & 0 & -E^1_{db} & 0 & -E^1_{dc} & -F^1_{dd} & 1 & -F^1_{de} & 0 & -F^1_{df} & 0 \\
0 & -E^2_{da} & -F^2_{db} & 0 & 0 & -E^2_{dc} & -F^2_{dd} & 1 & 0 & -E^2_{de} & -F^2_{df} & 0 \\
0 & -E^1_{ea} & 0 & -E^1_{eb} & 0 & -E^1_{ec} & -F^1_{ed} & 0 & -F^1_{ee} & 1 & -F^1_{ef} & 0 \\
0 & C^2_{ea} & D^2_{eb} & 0 & 0 & C^2_{ec} & D^2_{ed} & 0 & -1 & C^2_{ee} & D^2_{ef} & 0 \\
0 & -E^1_{fa} & 0 & -E^1_{fb} & 0 & -E^1_{fc} & -F^1_{fd} & 0 & -F^1_{fe} & 0 & -F^1_{ff} & 1 \\
0 & -E^2_{fa} & -F^2_{fb} & 0 & 0 & -E^2_{fc} & -F^2_{fd} & 0 & 0 & -E^2_{fe} & -F^2_{ff} & 1
\end{pmatrix}
\begin{pmatrix} q_a \\ u_a \\ q_b \\ u_b \\ q_c \\ u_c \\ q_d \\ u_d \\ q_e \\ u_e \\ q_f \\ u_f \end{pmatrix}
=
\begin{pmatrix} b^1_a \\ b^2_a \\ b^1_b \\ b^2_b \\ b^1_c \\ b^2_c \\ b^1_d \\ b^2_d \\ b^1_e \\ b^2_e \\ b^1_f \\ b^2_f \end{pmatrix}. \tag{24}$$

Although this system is never built explicitly, it is obvious that the GMRES algorithm will solve it in at most 12 iterations. It should also be clear by now, that each GMRES iterations amounts to the solution of one discrete problem in each of the subdomains, with the type of boundary conditions for each domain as previously selected and values as provided by the iterates of the interface variables.

We have thus arrived at a quite special domain decomposition methodology, in which we have significant freedom to introduce boundary conditions for each subdomain, without caring for what we are choosing for neighboring subdomains. Further, the iterative algorithm has the finite termination property; it converges in at most $2N$ iterations, where N is the number of interface nodes (we should mention, however, that this count does not always hold; when a node is shared by n subdomains, $n > 2$, the number of interface variables at this node is n and not 2).

We have not carried out detailed studies on this domain decomposition technique for 2D or 3D elliptic problems. We have however verified that the GMRES algorithm converges to the exact solution after $2N$ iterations, for any choice of boundary conditions for each subdomain. In the case of multiple 2D/3D subdomains, at each interface node there are as many interface unknowns as the number of subdomains sharing that node. The algorithm behaves much in the same way as in the 1D case, but obviously as N increases the burden of having multiple unknowns per interface node increases too. A detailed study, including the assessment of preconditioners, is left for future work.

On the other hand, there exist applications in which the number of coupling variables is always small, while flexibility in the imposition of boundary conditions and guaranteed convergence are essential. Such is the case of coupled, dimensionally–heterogeneous models, in which some parts of the simulation domain are modeled by complex 2D/3D subdomains, whereas others are simple enough to be accurately represented by 0D/1D approximations. We explore these applications in the next sections.

3. PARTITIONING OF COUPLED DIMENSIONALLY-HETEROGENEOUS MODELS

In this section the proposed strategy is used in the context of coupling models with different dimensionality, for which it was devised. For the sake of clarity, the presentation is restricted to the heat conduction problem with a single coupling interface in which a 3D model is coupled to a 1D model, as schematized in Figure 3.

A Dirichlet boundary condition $\bar{U}_2$ is applied over the rightmost boundary (see the hidden surface Γ_{D2} in the figure), and a value $\bar{U}_1$ is imposed at the leftmost point $z = b$. Over the rest of the boundary, denoted simply by Γ_R, a Robin boundary condition is assumed with

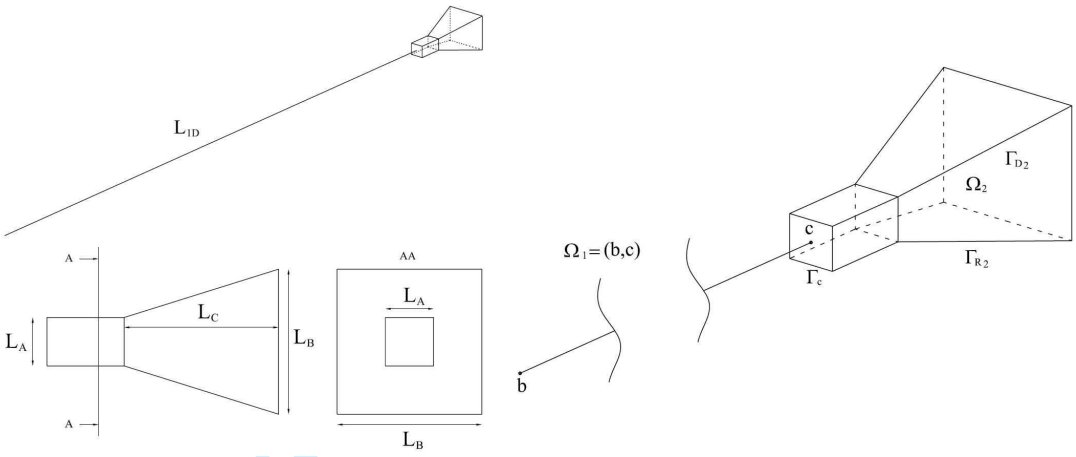

Figure 3. 3D–1D coupled models for the diffusion problem.

convection parameter h and environment temperature U_∞. Thus, it is $\Gamma_R = \Gamma_{R1} \cup \Gamma_{R2}$, whose outward unit normal is $\mathbf{n}$, where the boundary has been split into the corresponding parts to both subdomains. While the Robin condition is actually a boundary condition for the 3D domain over Γ_{R2}, it becomes a reaction term in the 1D submodel. For this latter submodel we need to specify the perimeter ϱ and cross sectional area A at each point z in the 1D domain. The dimensions that define the problem are denoted by L_{1D}, L_A, L_B and L_C, and are also specified in Figure 3. For this case of square section we have $A = L_A^2$ and $\varrho = 4L_A$.

The two subdomains are, thus, $\Omega_1 = (b, c)$, and Ω_2, which is the 3D domain shown in the figure. The coupling interface, denoted by Γ_c, is at $z = c$. It consists of a single point for the 1D model and of a square surface for the 3D model. The physics of the problem requires that continuity of temperature and heat flux hold, in an average sense, at Γ_c, leading to the

following problem for U_1 and U_2 (the solutions within each subdomain)

$$\begin{cases} -\dfrac{d}{dz}\left(kA\dfrac{dU_1}{dz}\right) + h\varrho U_1 = h\varrho U_\infty & \text{in } (b,c), \\ U_1(b) = \bar{U}_1, & \\ -\operatorname{div}(k\nabla U_2) = 0 & \text{in } \Omega_2, \\ U_2 = \bar{U}_2 & \text{on } \Gamma_{D2}, \\ hU_2 + k\nabla U_2 \cdot \mathbf{n} = hU_\infty & \text{on } \Gamma_{R2}, \\ U_1(c) = \dfrac{1}{A}\displaystyle\int_{\Gamma_c} U_2 \, d\Gamma & \text{at } z = c, \\ -kA\dfrac{dU_1}{dz}(c) = -\displaystyle\int_{\Gamma_c} k\nabla U_2 \cdot \mathbf{n} \, d\Gamma & \text{at } z = c, \end{cases} \tag{25}$$

where we have taken $\mathbf{n} = \mathbf{e}_z$ on Γ_c. The previous problem, however, is not well posed. Essentially, the coupling conditions on Γ_c (equations $(25)_6$ and $(25)_7$) are insufficient to make U_2 to be unique. The coupled formulation above leads to the so-called *defective boundary conditions* on Γ_c for Ω_2 [3, 4, 11, 12], which have also been studied in the framework of kinematically incompatible models [2, 7]. As a consequence, stronger conditions need to be enforced at Γ_c, and the choice is quite arbitrary as long as they are consistent with $(25)_6$–$(25)_7$. For the purpose of this example we choose to replace $(25)_7$ with the stronger pointwise condition

$$-k\frac{dU_1}{dz}(c) = -k\nabla U_2 \cdot \mathbf{n} \qquad \text{on } \Gamma_c, \tag{26}$$

which now leads to a well–posed problem. We point out that this choice is not linked to the methodology proposed in this article, which would work with any other well–posed formulation.

To apply the proposed strategy, the procedure is equivalent to that used in the first 1D/1D example, only that this time Ω_2 is 3D and the coupling variables are averages over Γ_c. We begin by defining q_c and u_c as the mean heat flux and temperature at the interface (Step 1).

Then we choose boundary conditions at Γ_c for each subdomain (Step 2). Since in the previous cases we have seen the Dirichlet–Neumann and Dirichlet–Dirichlet approaches, let us illustrate here the Neumann–Neumann approach, that is, $z = c$ is a Neumann boundary for both Ω_1 and Ω_2. To set up the system of equations for q_c and u_c (Step 3), we define the operators $\mathcal{U}_c^1$ and $\mathcal{U}_c^2$ as follows:

- Let w_γ be the solution of

$$\begin{cases} -\dfrac{d}{dz}\left(kA\dfrac{dw_\gamma}{dz}\right) + h\varrho w_\gamma = h\varrho U_\infty \quad \text{in } (b,c), \\ w_\gamma(b) = \bar{U}_1, \\ -k\dfrac{dw_\gamma}{dz}(c) = \gamma, \end{cases} \tag{27}$$

  and then we define, for any $\gamma \in \mathbb{R}$,

$$\mathcal{U}_c^1(\gamma) = w_\gamma(c). \tag{28}$$

- Let v_δ be the solution of

$$\begin{cases} -\operatorname{div}(k\nabla v_\delta) = 0 & \text{in } \Omega_2, \\ v_\delta = \bar{U}_2 & \text{on } \Gamma_{D2}, \\ hv_\delta + k\nabla v_\delta \cdot \mathbf{n} = hU_\infty & \text{on } \Gamma_{R2}, \\ -k\nabla v_\delta \cdot \mathbf{n} = \delta & \text{on } \Gamma_c, \end{cases} \tag{29}$$

  then we define, for any $\delta \in \mathbb{R}$,

$$\mathcal{U}_c^2(\delta) = \frac{1}{A}\int_{\Gamma_c} v_\delta \, d\Gamma. \tag{30}$$

Using these operators, we set up the system corresponding to Step 3, according to the proposed

methodology, which reads

$$\begin{aligned} r_1(q_c, u_c) &:= -\mathcal{U}_c^1(q_c) + u_c = 0, \\ r_2(q_c, u_c) &:= -\mathcal{U}_c^2(q_c) + u_c = 0, \end{aligned} \tag{31}$$

which can now be solved in 2 iterations with a matrix–free GMRES algorithm, exactly as done in Section 2.1. In fact, the only difference with Section 2.1 is that the operator $\mathcal{U}_c^2$ involves the solution of a 3D problem, but otherwise they are identical.

Remark 2. *In the 1D–1D example of Section 2.1, we were absolutely free to choose the boundary condition type for both subdomains. In the 1D–3D case, however, the situation is somewhat different. When the defective coupling conditions* $(25)_6$ *and* $(25)_7$ *are replaced by* $(25)_6$ *and* (26) *to get a well–posed problem, one of the consequences is that imposing the (mean) temperature on* Γ_c *for* Ω_2 *is no longer straightforward. In fact, it would be necessary to determine the operator* $\mathcal{Q}_c^2$*, defined by*

$$\mathcal{Q}_c^2(\gamma) = -\frac{1}{A}\int_{\Gamma_c} k\nabla v_\gamma \cdot \mathbf{n}\, d\Gamma, \tag{32}$$

where v_γ *is the unique solution of the well–posed, but non–standard, subproblem in* Ω_2 *given by:*

$$\begin{cases} -\operatorname{div}(k\nabla v_\gamma) = 0 & \text{in } \Omega_2, \\ v_\gamma = \bar{U}_2 & \text{on } \Gamma_{D2}, \\ hv_\gamma + k\nabla v_\gamma \cdot \mathbf{n} = hU_\infty & \text{on } \Gamma_{R2}, \\ -k\nabla v_\gamma \cdot \mathbf{n} = p & \text{on } \Gamma_c, \\ \dfrac{1}{A}\displaystyle\int_{\Gamma_c} v_\gamma\, d\Gamma = \gamma & \text{on } \Gamma_c. \end{cases} \tag{33}$$

where $p \in \mathbb{R}$ *is the unique constant that makes the mean value of* v_γ *over* Γ_c *to coincide with* γ*. Clearly, most available 3D codes do not offer such boundary conditions as a ready-to-use*

option. In fact, if one wants Γ_c *to be a Dirichlet boundary for* Ω_2*, it is simpler to set up another well–posed problem imposing the following coupling conditions (again consistent with* $(25)_6$ *and* $(25)_7$*)*

$$U_1(c) = U_2 \qquad \text{on } \Gamma_c \tag{34}$$

$$-kA\frac{dU_1}{dz}(c) = -\int_{\Gamma_c} k\nabla U_2 \cdot \mathbf{n}\, d\Gamma \qquad \text{at } z = c, \tag{35}$$

so that U_2 *is constrained to be constant over* Γ_c*. In this case, the definition of* $\mathcal{Q}_c^2$ *remains given by* (32)*, but now* v_γ *is the solution of the standard problem*

$$\begin{cases} -\operatorname{div}(k\nabla v_\gamma) = 0 & \text{in } \Omega_2, \\ v_\gamma = \bar{U}_2 & \text{on } \Gamma_{D2}, \\ hv_\gamma + k\nabla v_\gamma \cdot \mathbf{n} = hU_\infty & \text{on } \Gamma_{R2}, \\ v_\gamma = \gamma & \text{on } \Gamma_c. \end{cases} \tag{36}$$

As said, a discussion about the choice of the specific coupling conditions is outside the scope of this study. Notice for example that the constant profile for U_2 *over* Γ_c *could be replaced by any other.*

In the same spirit as with the example of Section 2, let us give the iterations of the GMRES algorithm explicitly, starting with the initial condition $X_0 = (q_c^0, u_c^0) = (1, 10)$. The constants that define the problem are set to $L_{1D} = 1000$, $L_A = 25$, $L_B = 75$, $L_C = 80$, $\varrho = 100$, $A = 625$, $\bar{U}_1 = 0$, $\bar{U}_2 = 10$, $U_\infty = 1$, $k = 1$ and $h = 0.001$. Hence, we have

$$r(X_0) = \begin{pmatrix} 87.8470 \\ -68.0409 \end{pmatrix}, \qquad v_1 = \begin{pmatrix} 0.7906 \\ -0.6123 \end{pmatrix},$$

to calculate $r(X_0)$ we needed to solve a 1D problem over Ω_1 with Neumann boundary condition and a 3D problem over Ω_2 also with Neumann boundary condition, both given by q_c^0. As before,

to calculate $r(X_0+v_1)$ we solve a 1D problem over Ω_1 and a 3D problem both with Neumann conditions given by the component $(X_0+v_1)_1 = 1.7906$, yielding

$$w_1 = \begin{pmatrix} -61.7234 \\ 54.4049 \end{pmatrix}, \qquad H_{11} = (w_1, v_1) = -82.1125,$$

$$w_1 = w_1 - H_{11}v_1 = \begin{pmatrix} 3.1941 \\ 4.1238 \end{pmatrix}, \qquad H_{21} = 5.2161,$$

$$v_2 = \begin{pmatrix} 0.6123 \\ 0.7906 \end{pmatrix}.$$

We now calculate $r(X_0 + v_2)$ imposing, again, Neumann boundary conditions for Ω_1 (1D problem) and for Ω_2 (3D problem), both given by $(X_0 + v_2)_1$. Once more, note that the GMRES algorithm provides the right amount of information, through the orthogonalization process, in order to ensure convergence in two iterations. Finally, we reach the following system to compute the minimizer in the GMRES algorithm

$$\begin{pmatrix} 6769.6770 & 5252.6326 \\ 5252.6326 & 4078.7397 \end{pmatrix} \begin{pmatrix} y_1 \\ y_2 \end{pmatrix} = \begin{pmatrix} -9123.9729 \\ -7091.9270 \end{pmatrix} \quad \Rightarrow \quad y = \begin{pmatrix} 1.7138 \\ -3.9458 \end{pmatrix},$$

leading to

$$X_2 = X_0 + y_1v_1 + y_2v_2 = \begin{pmatrix} -0.0612713 \\ 5.8310468 \end{pmatrix} = \begin{pmatrix} q_c \\ u_c \end{pmatrix},$$

that is the exact result in the sense of the result we would obtain using a monolithic approach.

The final result is shown in Figure 4 together with some details of the solution over the 3D domain. In these figures the 1D domain has been plotted as the 3D domain that it actually represents. Note that the constant temperature across the transversal section of the 1D model is a good approximation when compared with the temperature of the 3D region at the interface. The transversal plane with opacity corresponds to the coupling interface between sub-domains.

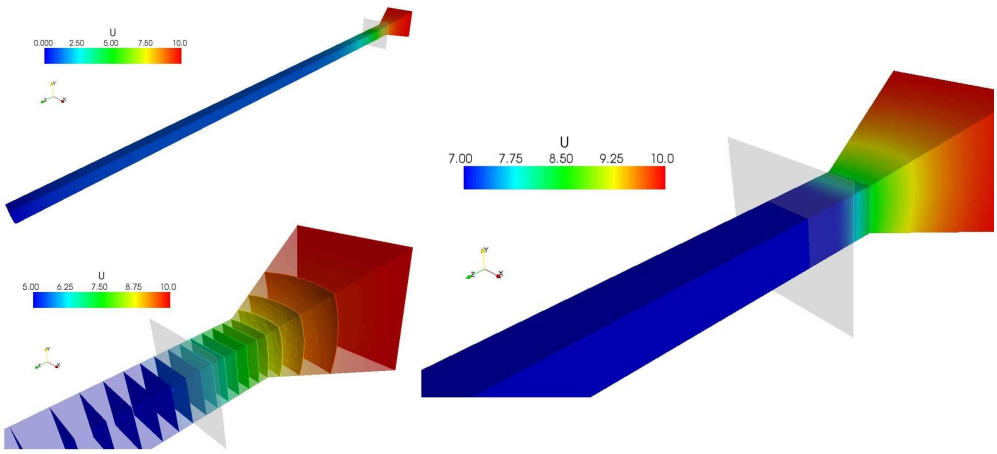

Figure 4. Results for the 3D–1D coupled problem.

4. NUMERICAL RESULTS

In this section we present two examples whose main aim is to show the potential of the partitioning strategy described in the previous sections in more complex situations.

4.1. Satellite-like geometrical structure

In this first example we couple a 3D spherical structure with twenty–four 1D models that represent a set of cylinders attached to it. The whole structure reminds an old-fashioned satellite. In Figure 5 the full domain is presented, together with its approximation with 1D models replacing the cylinders.

The problem consists of a diffusion problem with a Robin boundary condition over the whole surface except for each one of the free extremes of the set of pipes (the surfaces of the cylinders whose normal vector is pointing outwards), where an homogeneous Neumann boundary condition was considered. Therefore, in this problem we do not have Dirichlet

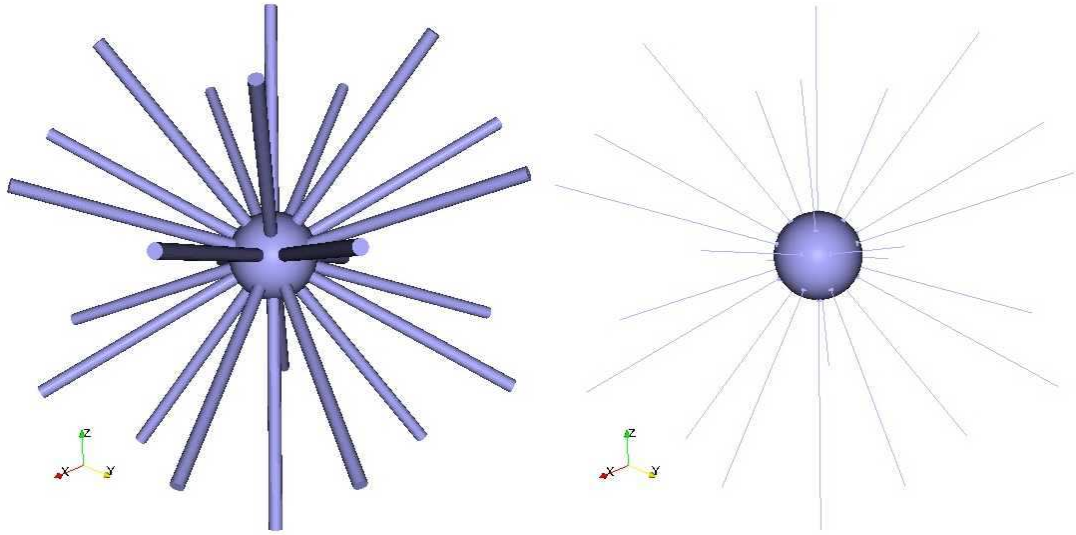

Figure 5. 3D mechanism for heat transfer and approximate 3D–1D model.

boundary. Basically, the problem is the same as the one tackled in Section 3. In addition, here we consider a constant volume source f acting in the whole domain. For the sake of brevity we do not repeat the mathematical statement of the problem. The problem is characterized by the radius of the sphere R_s and the radius of each cylinder R_c. The length of each pipe is denoted by L. There are three pipes per octant. In the first octant (all coordinates positive) the directors corresponding to the pipes are $\frac{1}{\sqrt{6}}(2,1,1)$, $\frac{1}{\sqrt{6}}(1,2,1)$ and $\frac{1}{\sqrt{6}}(1,1,2)$. For the other octants the pipes are placed analogously. Hence, the coupled 3D–1D model consists of 24 coupling interfaces grouped in the set $\Sigma = \{(\Gamma_{ci})_{i=1,\dots,24}\}$ for which two unknowns are defined over each interface. Then, our problem is of dimension 48 (mean temperature and heat flux are the interface unknowns). Figure 6 presents a detail of the mesh over a portion of the domain and the part of the surface that corresponds to the interface with the 1D submodel.

Recalling the physical parameters involved (see Section 3), the problem is characterized by

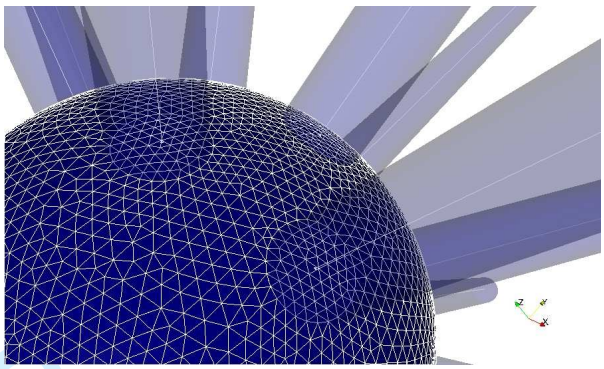

Figure 6. Detail of mesh over the coupling interfaces.

$L = 5$, $R_s = 1$, $R_c = 0.15$, $\varrho = 0.942478$, $A = 0.070686$, $U_\infty = 10$, $k = 1$, $f = 0.1$ and $h = 0.01$. The Biot number of the cylinders is $Bi = hR_c/k = 0.0015 << 1$, indicating that in each cylinder the exact solution is indeed almost constant over each cross section [15].

Each interface entails the coupling of approximately 70 nodes from the 3D model with a single node from the 1D model. And this structure is repeated 24 times. For this problem we considered Neumann boundary conditions for all the boundaries, from both models, that are involved in the coupling. Finally, the last step (Step 4) requires to choose an iterative algorithm for the resolution of this problem. Again, the matrix–free GMRES algorithm was employed. The results are presented in Figure 7. The color scales were manipulated to capture the variation of the solution in the 3D sphere. Also, the convergence history of the iterative process is shown in Figure 8 in logarithmic scale. Although we have the convergence assured by the algorithm, observe that the residual is reduced by 8 orders of magnitude after 4 to 5 iterations, which is enough to reach reasonable results according to the tolerances usually used in this kind of computation.

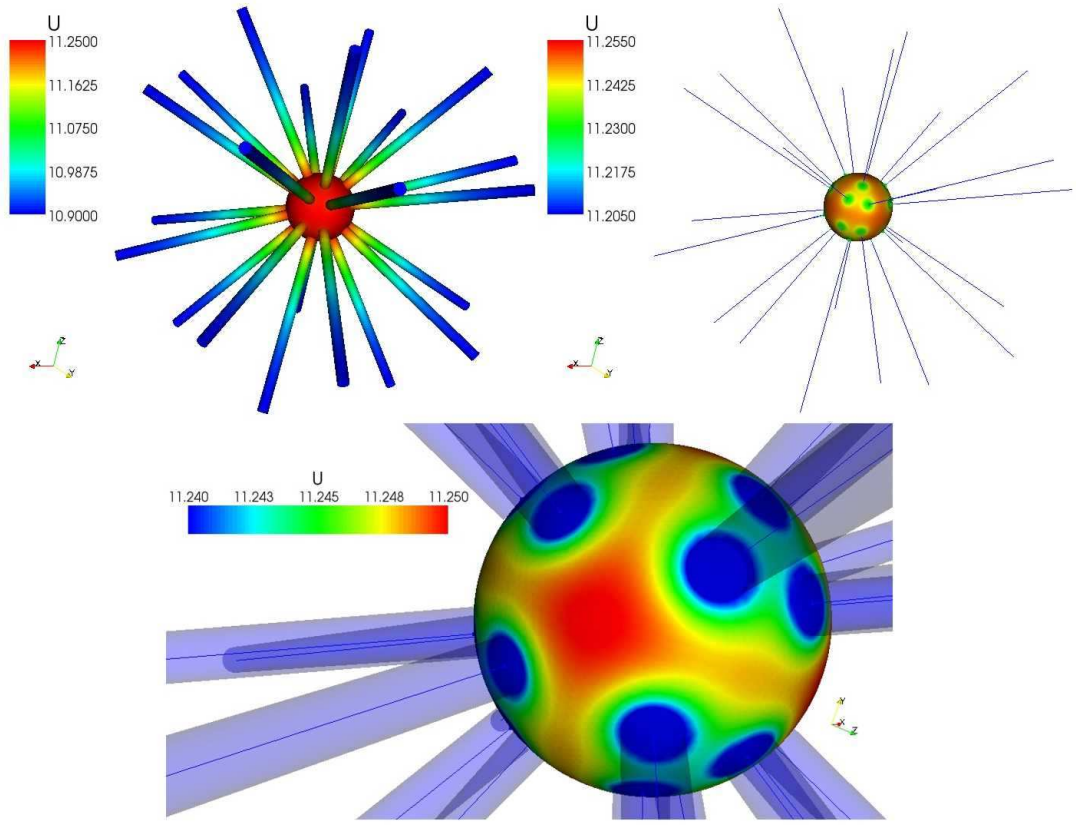

Figure 7. Results for the satellite-like mechanism.

4.2. Double helix geometrical structure

This second example is an even more complex situation in terms of the number of coupling variables in the problem. Here we employ a geometrical pattern that resembles a DNA double helix structure, and we solve a heat transfer problem like the one presented in Section 3 by replacing some parts of the 3D model with 1D representations. The domain is shown in Figure 9, where it can be seen that the inter-helix connections have been replaced by 1D simplified representations (the helices are modeled through 3D models).

For this heat transfer problem Robin boundary conditions over the whole surface are

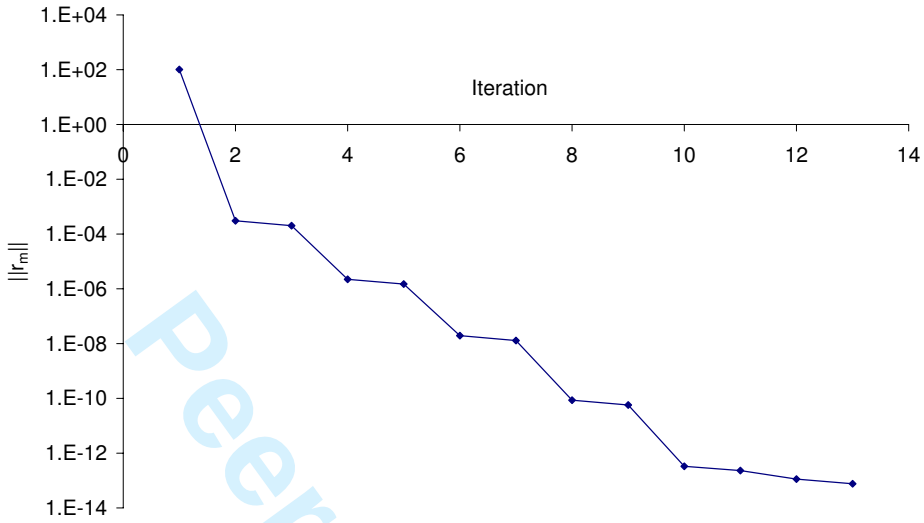

Figure 8. Convergence history of the residual $r_m = r(X_m)$ for the satellite-like mechanism.

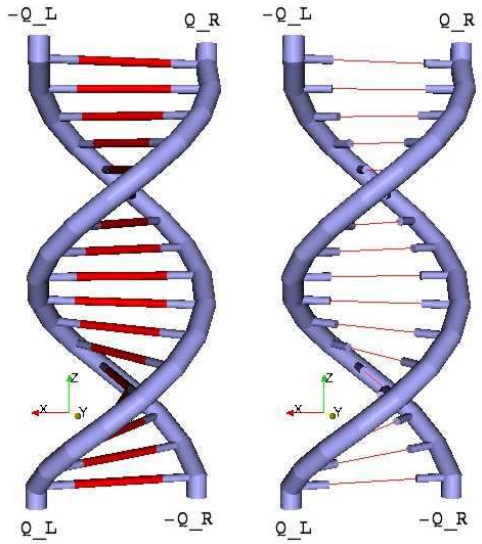

Figure 9. 3D mechanism for heat transfer and approximate 3D–1D model.

imposed, except for the ends of the helices, at which Neumann boundary conditions (imposed heat fluxes) are applied (see Figure 9). The connections are denoted by c_i, $i = 1, \ldots, 17$, being c_1 the lowermost connection and c_{17} the uppermost. The volumetric heat source is of value f in the domains corresponding to the 1D connections c_i, $i = 8, 9, 10$, and null elsewhere. Finally, the value of the conductivity for the helices is k_h, while for the connections it is k_{c_i}, $i = 1, \ldots, 17$.

The problem is also characterized by the distance between helices D_h, the radius of the helices R_c, the radius of each inter-helix connection r_c, the length of each 1D model L_{1D}, the vertical spacing between connections L_c, the height of the structure L_h and the angle between two consecutive connections, denoted by θ. The imposed heat fluxes at the ends of the helices are $\bar{Q}_L$, $-\bar{Q}_L$, $\bar{Q}_R$ and $-\bar{Q}_R$, as sketched in Figure 9. The actual values used for the parameters are: $D_h = 4$, $R_c = 0.25$, $r_c = 0.1$, $L_{1D} = 2.2$, $L_c = 0.625$, $L_h = 12$, $\theta = 22.5$, $\varrho = 0.6283$, $A = 0.031416$, $f = 1$, $h = 0.01$, $U_\infty = 1$, $k_h = 1$, $k_{c_i} = 3$, for i odd and $k_{c_i} = 1$, for i even. The problem is solved considering all the interfaces in the problem as Neumann boundaries.

The coupled 3D–1D model consists of 34 coupling interfaces, so we have in this case that $\Sigma = \{(\Gamma_{ci})_{i=1,\ldots,34}\}$.Since the problem is completely described by means of two unknowns per interface, our problem has dimension 68. Figure 10 gives a detail of the internal part of the structure and of the mesh used in the computations.

As in the example of Section 4.1, Step 1 of the proposed strategy was accomplished by defining two variables (mean temperature and mean heat flux) over each coupling interface, $q_i's$ and $u_i's$, $i = 1, \ldots, 34$. Step 2 was performed by selecting Neumann boundary conditions for each subdomain at the coupling interfaces. The defective boundary conditions were supplemented with the condition that the heat flux is constant over each interface, which

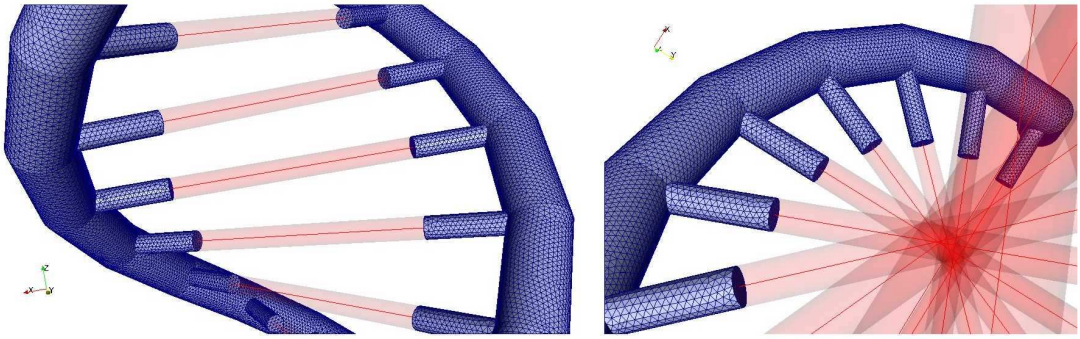

Figure 10. Details of the structure and mesh.

is the simplest choice for Neumann boundaries. Step 3 consisted of setting up the system of 68 equations, which is straightforward. To complete the process we have to perform Step 4, that is selecting an iterative procedure for solving the linear system. As in all the examples in this study, the free-matrix version of the GMRES algorithm was employed for the resolution of this problem. Therefore, the procedure guarantees the convergence, to the solution we would obtain with a monolithic approach, after 68 iterations.

Remark 3. *Notice that the 3D models are actually decoupled from one another and they are solved separately at each iteration.*

The results of the simulation are presented in Figure 11. As with the previous example, for plotting purposes, the 1D model is replaced by a 3D model (but the solution obviously corresponds to the former). A detail of the solution is also included in Figure 12 by manipulating the scale to be able to notice the pattern of the solution in the middle part of the structure where the source term is acting. These results are mere illustrations of the proposed technique, so that they will not be further discussed. The convergence history of the iterative procedure is presented in Figure 13 in logarithmic scale. In this case, the residual is

reduced by 6 orders of magnitude after 24 to 25 iterations, reaching satisfactory results without the need of performing all the 68 iterations hypothetically required by the GMRES algorithm to guarantee convergence.

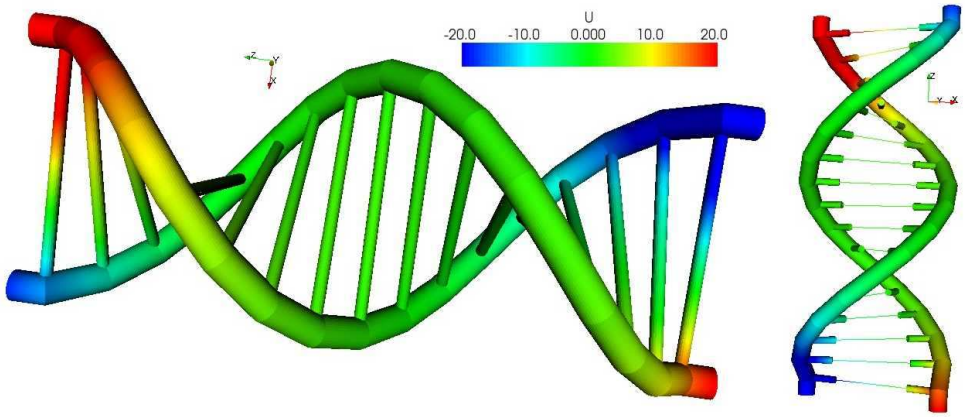

Figure 11. Results for the DNA-like mechanism.

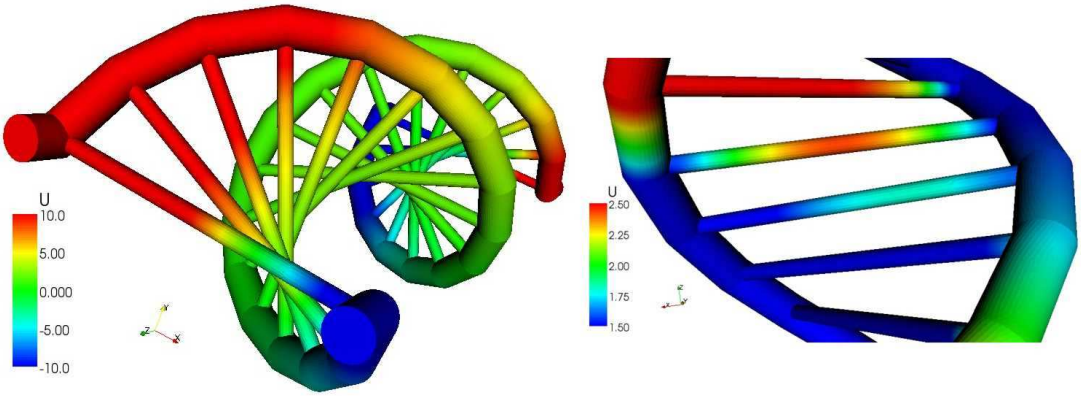

Figure 12. Details of the solution in the DNA-like mechanism.

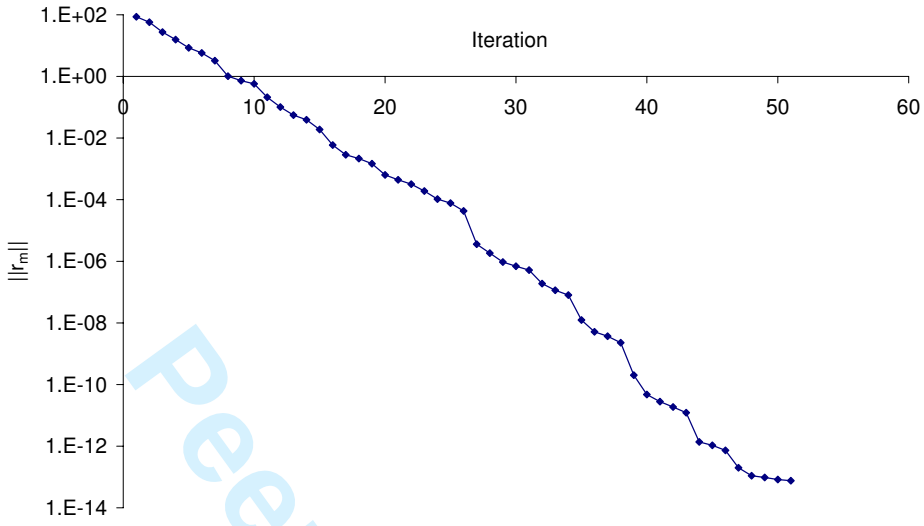

Figure 13. Convergence history of the residual $r_m = r(X_m)$ for the DNA-like mechanism.

5. ADDITIONAL REMARKS ON THE COUPLING STRATEGY

This section presents a series of remarks including the possibility of adopting Robin boundary conditions at the interface, and of addressing time-dependent and non-linear problems.

5.1. On Robin boundary conditions

Up to now we have considered either Dirichlet or Neumann boundary conditions at the coupling interface Γ_c. In some cases it is preferrable to impose Robin conditions, i.e., to impose the value of a linear combination $\alpha u + \beta \nabla u \cdot \mathbf{n}$. Some reasons to do this are:

(i) When the subdomain has no Dirichlet boundary; in which case imposing Neumann conditions at the coupling interface leads to an ill–posed problem. This difficulty may be tackled by choosing a Robin boundary condition at the coupling interface, with a small value of α [16].

(ii) When there is a convection field $\mathbf{v}$ across Γ_c, the continuity of the total flux $(-k\nabla u+\mathbf{v}u)\cdot\mathbf{n}$ needs to be ensured to have conservation, leading to a Robin condition. In particular, this is crucial when one of the subdomains has a zero diffusion coefficient [17].

(iii) Robin boundary conditions may also prove useful to get a better-conditioned global system, as proposed recently by [18] for fluid–structure interaction.

Let us sketch how these conditions can be treated within the proposed strategy going back to the problem of Section 3. Consider that the relevant physics imposes the continuity of a linear combination $\alpha u + \beta\nabla u\cdot\mathbf{n}$ at Γ_c, where α and β are scalars ($\beta\neq 0$) that vary in space (and thus from subdomain to subdomain). Hence, the minimal coupling conditions emanating from the physics are, instead of $(25)_6$–$(25)_7$,

$$\alpha_1(c)U_1(c)+\beta_1(c)\frac{dU_1}{dz}(c)=\frac{1}{A}\int_{\Gamma_c}\left(\alpha_2U_2+\beta_2\nabla U_2\cdot\mathbf{n}\right)d\Gamma \qquad \text{on } \Gamma_c, \tag{37}$$

$$U_1(c)=\frac{1}{A}\int_{\Gamma_c}U_2\,d\Gamma \qquad \text{on } \Gamma_c, \tag{38}$$

where the subindices added to α and β denote the subdomain. These conditions are again insufficient to completely determine the problem (defective boundary conditions). We have to strengthen one of the previous equations, and for Robin boundary conditions on Γ_c for Ω_2 it is natural to replace (37) by its pointwise version

$$\alpha_1U_1+\beta_1\frac{dU_1}{dz}=\alpha_2U_2+\beta_2\nabla U_2\cdot\mathbf{n} \qquad \text{on } \Gamma_c, \tag{39}$$

The interface variables are now selected as f_c and u_c, the average values over Γ_c of $\alpha u+\beta\nabla u\cdot\mathbf{n}$ and u, respectively. We keep $z=c$ as Neumann boundary for Ω_1, as in Section 3, so that the operator $\mathcal{U}_c^1$ remains as in (28). Notice that, for a given value of f_c and u_c, the diffusion flux q_c approaching $z=c$ from the left is given by

$$q_c(f_c,u_c)=-\frac{k}{\beta_1}\left(f_c-\alpha_1u_c\right). \tag{40}$$

The equation supplied by Ω_1, in terms of f_c and u_c, is thus (instead of the first equation of (31))

$$r_1(f_c, u_c) := -\mathcal{U}_c^1\left(-\frac{k}{\beta_1}(f_c - \alpha_1 u_c)\right) + u_c = 0. \tag{41}$$

To build the equation supplied by Ω_2, let v_ξ be the solution of

$$\begin{cases} -\operatorname{div}(k\nabla v_\xi) = 0 & \text{in } \Omega_2, \\ v_\xi = \bar{U}_2 & \text{on } \Gamma_{D2}, \\ hv_\xi + k\nabla v_\xi \cdot \mathbf{n} = hU_\infty & \text{on } \Gamma_{R2}, \\ \alpha_2 v_\xi + \beta_2 \nabla v_\xi \cdot \mathbf{n} = \xi & \text{on } \Gamma_c. \end{cases} \tag{42}$$

We assume that the scalars α_2 and β_2 render the above problem well posed. Then we define, for any $\xi \in \mathbb{R}$,

$$\mathcal{R}_c^2(\xi) = \frac{1}{A}\int_{\Gamma_c} v_\xi \, d\Gamma. \tag{43}$$

Using this operator, the second equation of the system reads

$$r_2(f_c, u_c) := -\mathcal{R}_c^2(f_c) + u_c = 0, \tag{44}$$

which together with (41) completes the closed system to which the iterative method is to be applied.

5.2. Extension to non-linear problems

Let us now go back to the problem of Section 3 and consider a nonlinear variant, as would happen, for example, if the thermal conductivity k is a function of the temperature u. In fact, the strategy can be applied in exactly the same way as for the linear case, arriving at the system of equations (31). The novelty, however, is that now the operators $\mathcal{U}_c^1$ and $\mathcal{U}_c^2$ are nonlinear. As a consequence, the matrix-free GMRES algorithm described in Section 2 no longer applies.

There exist, however, matrix-free nonlinear solvers, of which we have experimented the GMRES Krylov-Newton method (as detailed in [19]) and several Quasi-Newton methods (variants of Broyden's secant updates method) for non-symmetric systems [20]. In our experience, which is not reported here for brevity, all of these methods behave similarly, and in particular exhibit convergence to the solution of the coupled problem in a robust way.

5.3. Transient problems

If the problem under study evolves in time, temporal discretization by finite differences (or other technique) turns it into a sequence of (possibly nonlinear) problems of the kind already addressed in the previous sections. Implementation details and numerical tests of the proposed strategy on transient, non-linear problems are the subject of a forthcoming article (see also [21]). Both Krylov-type and Broyden-type methods exhibit convergent behavior and can be applied without difficulty. Notice that, since the coupled system is solved until convergence, the order of the time-discretization is not affected by treating the sub-domains separately.

It is also worth noting that the change in the type of boundary condition applied to a particular interface of a subdomain implies only changing one equation in the coupled system. This could be done at each time step according to the more appropriate kind of boundary condition to be applied, which could vary from time step to time step. An instance of this is the case of hyperbolic problems with dynamic boundary conditions.

A useful remark concerning transient problems is that the variants of Broyden's method, which along the iterations update an approximation $\mathsf{B}^{(k)}$ of the Jacobian matrix, tend to be more effective. In fact, at each time step the approximate Jacobian needs to be initialized, and choosing the last $\mathsf{B}^{(k)}$ of the previous time step as $\mathsf{B}^{(0)}$ for the current one turns out to be an

excellent choice. Even in complex nonlinear coupled problems using this strategy we obtained convergence in two to four iterations at each time step.

6. CONCLUSIONS

This work dealt with the development of a novel partitioned coupling procedure to tackle the coupled solution of dimensionally-heterogeneous models. The procedure is based on the quite simple idea of recasting the strongly-coupled problem in such a way that the popular Dirichlet-to-Neumann domain decomposition method becomes nothing but the application of Gauss–Seidel iterations to a suitably-defined (linear or nonlinear) system of equations. Notice that the D-to-N method coincides with the most widely used coupling method in fluid-structure interaction (i.e., transferring forces from the fluid to the structure, and displacements, or velocities, from the structure to the fluid). The same framework can thus also be applied in fluid-structure interaction.

Once the interface variables and equations are suitably defined, our investigation follows the natural path of replacing the Gauss–Seidel method with other, well-established, iterative methods. It has been shown that GMRES leads to rapid convergence in the reported examples. Though they will be reported in a future communication, we anticipate that the benefits are even larger in transient, nonlinear problems.

The proposed methodology treats each subsystem as a blackbox, in which the only restriction to the boundary conditions is that they lead to a well-posed problem. In this way, much freedom is gained since the boundary conditions imposed on each side of each interface can be chosen independently.

Further, the rapid convergence, together with the finite termination property in linear (or

linearized) systems, guarantee that instabilities arising from the coupling procedure can be avoided. In fact, the proposed methodology solves the strongly coupled system in a few iterations and independently of any elusive relaxation factor. Robust, automatic strategies based on blackbox codes, suitable for large-scale engineering applications, become in this way feasible.

ACKNOWLEDGEMENTS

This work was partially supported by the Brazilian agencies FAPESP, FAPERJ and CNPq, and by the Argentine agency ANPCyT. The support of these agencies is gratefully acknowledged.

REFERENCES

1. Felippa C, Park K, Farhat C. Partitioned analysis of coupled mechanical systems. *Comp. Meth. Appl. Mech. Engrg.* 2001; **190**:3247–3270.
2. Blanco P, Feijóo R, Urquiza S. A unified variational approach for coupling 3D–1D models and its blood flow applications. *Comp. Meth. Appl. Mech. Engrg.* 2007; **196**:4391–4410.
3. Formaggia L, Gerbeau JF, Nobile F, Quarteroni A. Numerical treatment of defective boundary conditions for the Navier–Stokes equations. *SIAM J. Num. Anal.* 2002; **40**:376–401.
4. Formaggia L, Gerbeau J, Nobile F, Quarteroni A. On the coupling of 3D and 1D Navier–Stokes equations for flow problems in compliant vessels. *Comp. Meth. Appl. Mech. Engrg.* 2001; **191**:561–582.
5. Urquiza S, Blanco P, Vénere M, Feijóo R. Multidimensional modelling for the carotid artery blood flow. *Comp. Meth. Appl. Mech. Engrg.* 2006; **195**:4002–4017.
6. Aufranc M. Numerical study of a junction between a three–dimensional elastic structure and a plate. *Comp. Meth. Appl. Mech. Engrg.* 1989; **74**:207–222.
7. Blanco P, Feijóo R, Urquiza S. A variational approach for coupling kinematically incompatible structural models. *Comp. Meth. Appl. Mech. Engrg.* 2008; **197**:1577–1602.

8. Ciarlet P, Dret HL, Nzengwa R. Junctions between three–dimensional and two–dimensional linearly elastic structures. *J. Math. Pures Appl.* 1989; **68**:261–295.
9. Kozlov V, Maz'ya V, Movchan A. Fields in non-degenerate 1D–3D elastic multi-structures. *Quart. J. Mech. Appl. Math.* 2001; **54**:177–212.
10. Deparis S, Discacciati M, Fourestey G, Quarteroni A. Fluid–structure algorithm based on Steklov–Poincaré operators. *Comp. Meth. Appl. Mech. Engrg.* 2006; **195**:5797–5812.
11. Veneziani A, Vergara C. An approximate method for solving incompressible Navier–Stokes problems with flow rate conditions. *Comp. Meth. Appl. Mech. Engrg.* 2007; **196**:1685–1700.
12. Veneziani A, Vergara C. Flow rate defective boundary conditions in haemodynamics simulations. *Int. J. Num. Meth. Fluids* 2005; **47**:803–816.
13. Park K, Felippa C. A variational principle for the formulation of partitioned structural systems. *Int. J. Num. Meth. Engng.* 2000; **47**:395–418.
14. Matthies H, Niekamp R, Steindorf J. Algorithms for strong coupling procedures. *Comp. Meth. Appl. Mech. Engrg.* 2006; **195**:2028–2049.
15. Incropera F, DeWitt D. *Introduction to Heat Transfer*. J. Wiley and Sons, 1985.
16. Houzeaux G, Codina R. An overlapping iteration-by-subdomain Dirichlet/Robin domain decomposition method for advection-diffusion problems. *Journal of Computational and Applied Mathematics* 2003; **158**:243–276.
17. Quarteroni A, Valli A. *Domain Decomposition Methods for Partial Differential Equations*, vol. Chapter 8. Oxford University Press, 1999.
18. Nobile F, Vergara C. An effective fluid-structure interaction formulation for vascular dynamics by generalized Robin conditions. *SIAM J. Sci. Comput.* 2008; **30**:731–763.
19. Kelley C. *Iterative Methods for Linear and Nonlinear Equations*, vol. Chapter 6. Frontiers in applied mathematics, SIAM, 1995.
20. Dennis J, Schnabel R. *Numerical Methods for Unconstrained Optimization and Nonlinear Equations*, vol. Chapter 8. Classics in applied mathematics, SIAM, 1996.
21. Leiva J. In preparation. PhD Thesis, Instituto Balseiro, Bariloche 2009.

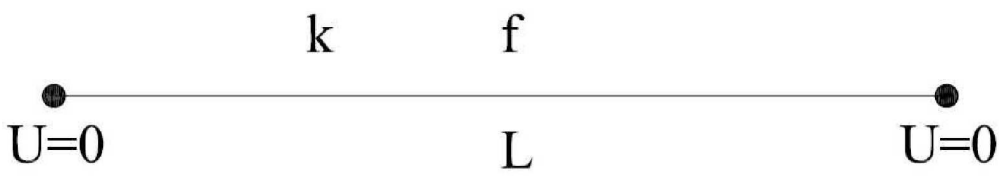

Diffusion problem in a 1D domain
334x57mm (600 x 600 DPI)

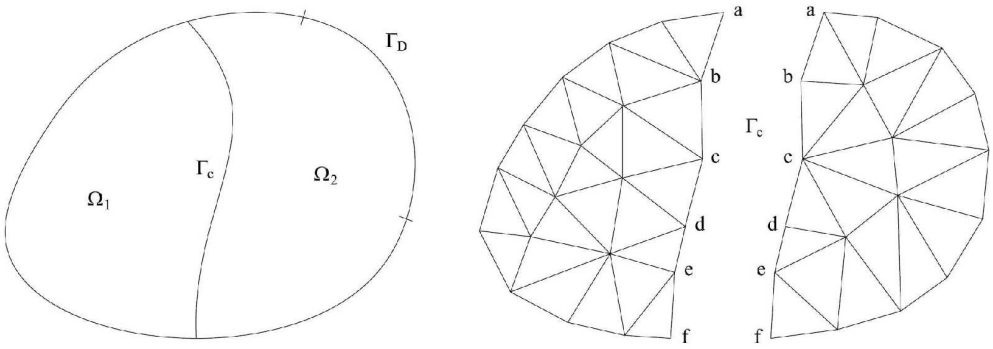

(a) Partitioning of the domain. (b) Meshes for both partitions.

Diffusion problem in a 2D domain
681x275mm (600 x 600 DPI)

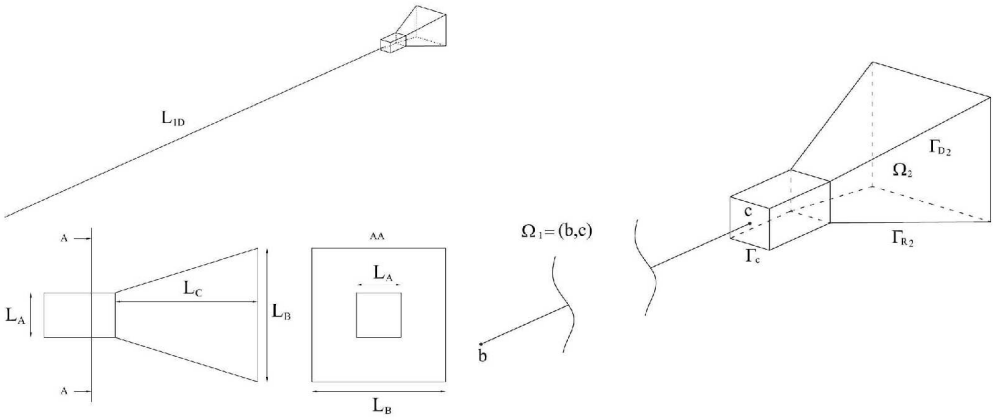

3D-1D coupled models for the diffusion problem
748x316mm (600 x 600 DPI)

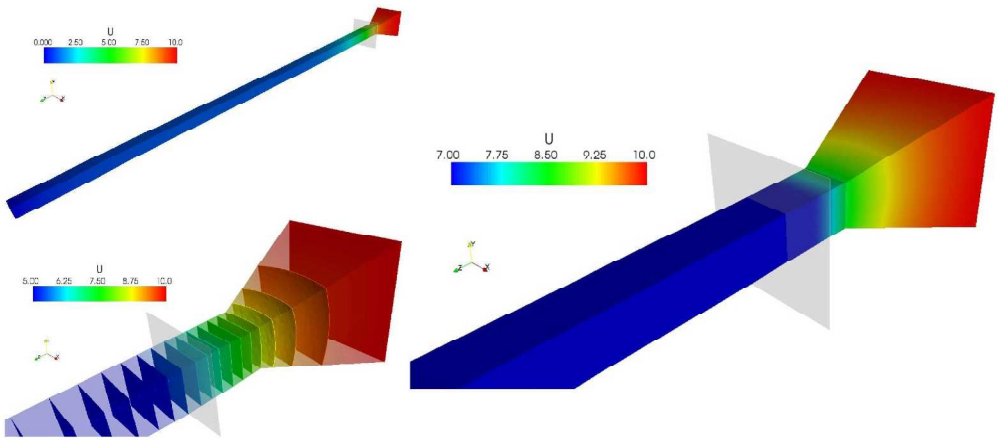

Results for the 3D-1D coupled problem
870x384mm (600 x 600 DPI)

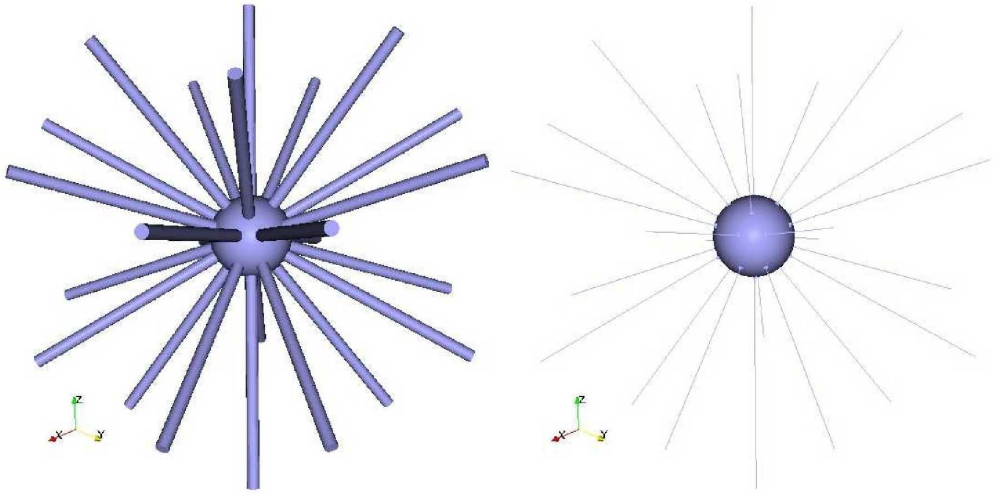

3D mechanism for heat transfer and approximate 3D-1D model
383x191mm (600 x 600 DPI)

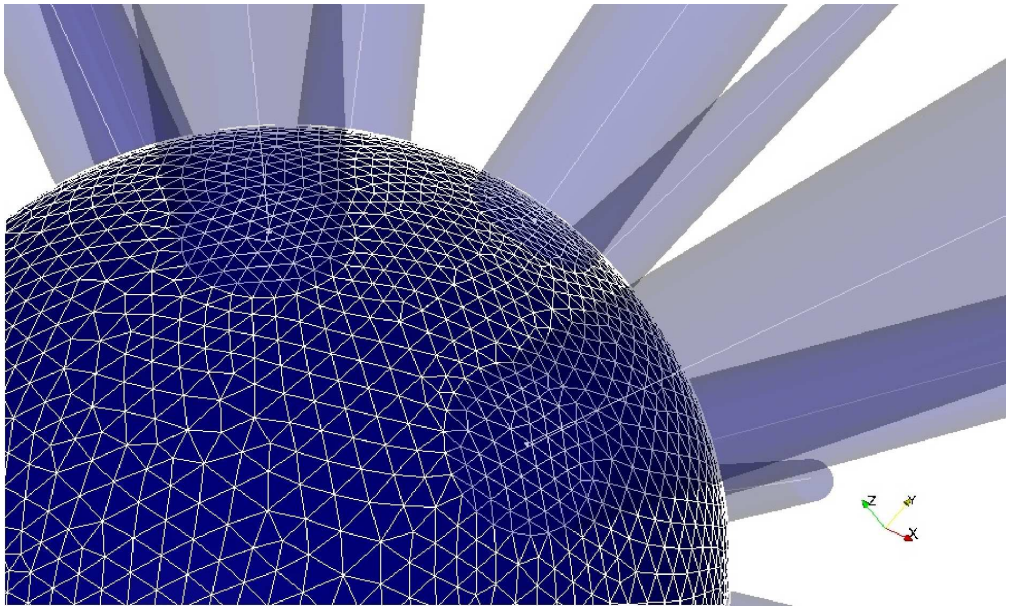

Detail of mesh over the coupling interfaces
316x190mm (600 x 600 DPI)

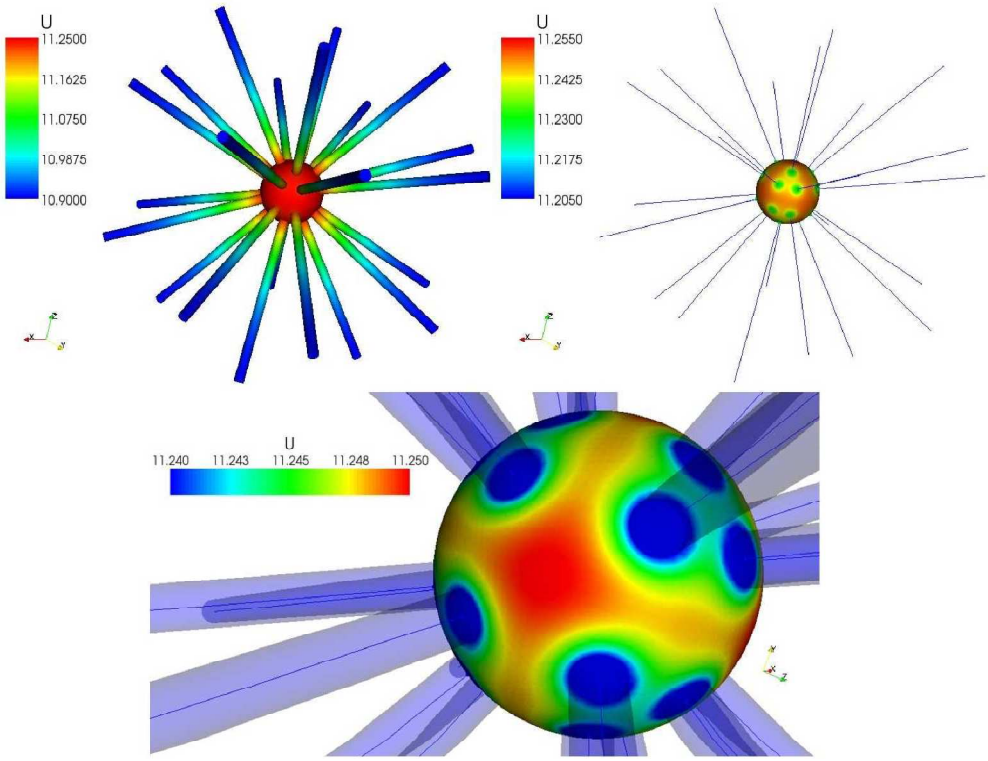

Results for the satellite-like mechanism
498x381mm (600 x 600 DPI)

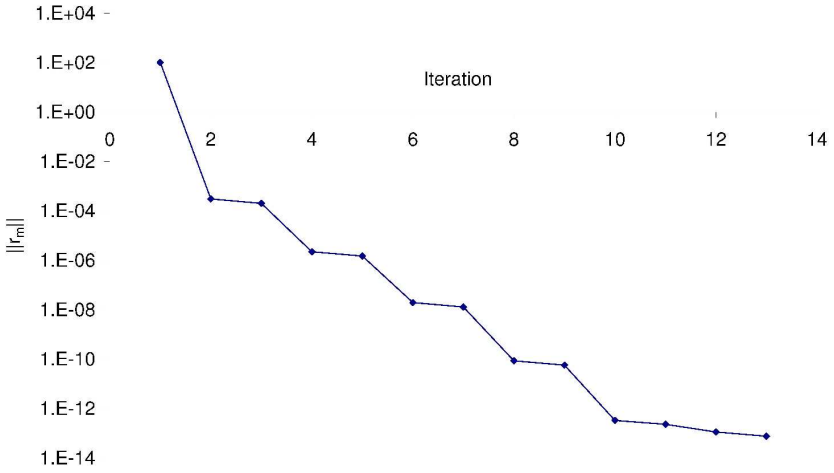

Convergence history of the residual $r_m=r(X_m)$ for the satellite-like mechanism
297x209mm (600 x 600 DPI)

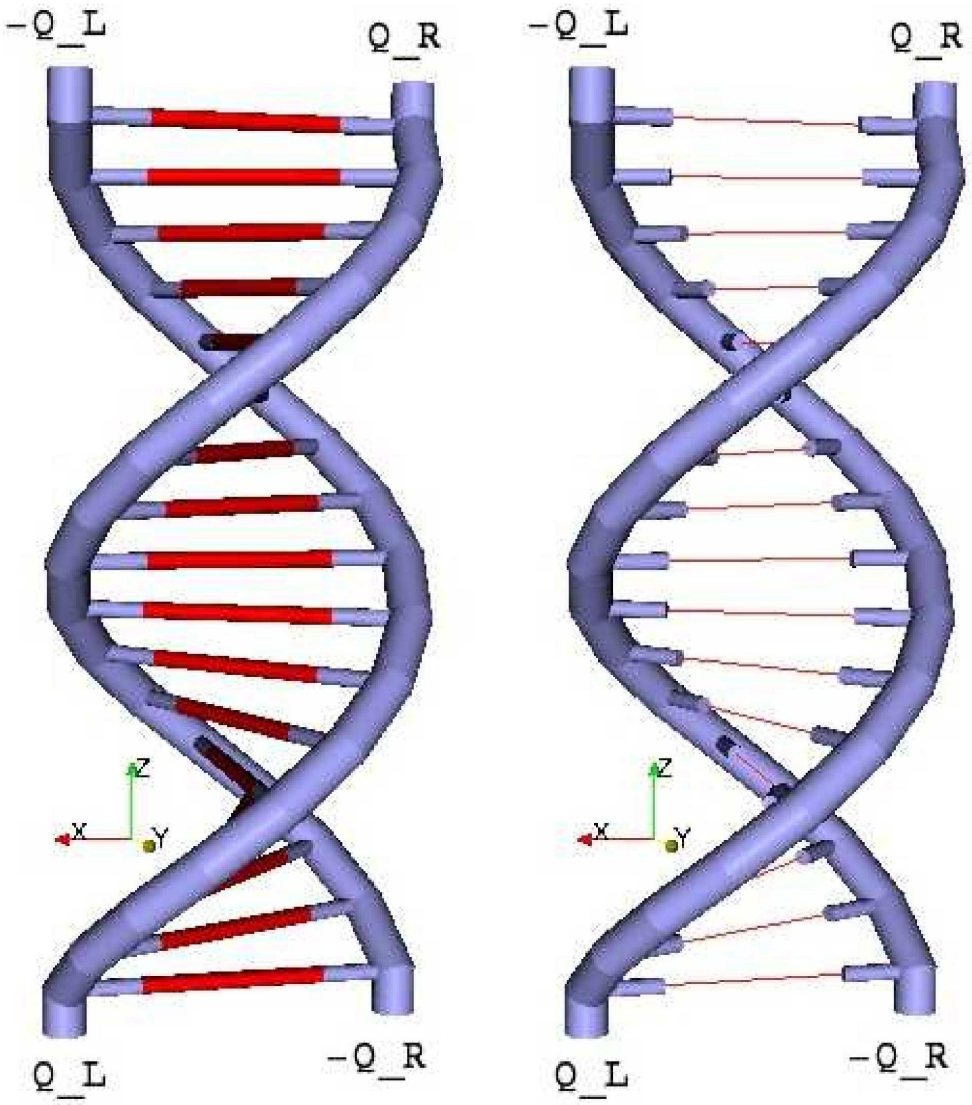

3D mechanism for heat transfer and approximate 3D-1D model
168x190mm (600 x 600 DPI)

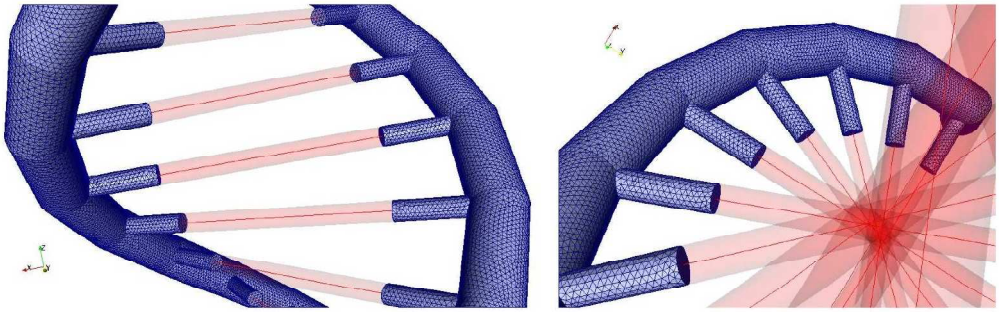

Details of the structure and mesh
628x196mm (600 x 600 DPI)

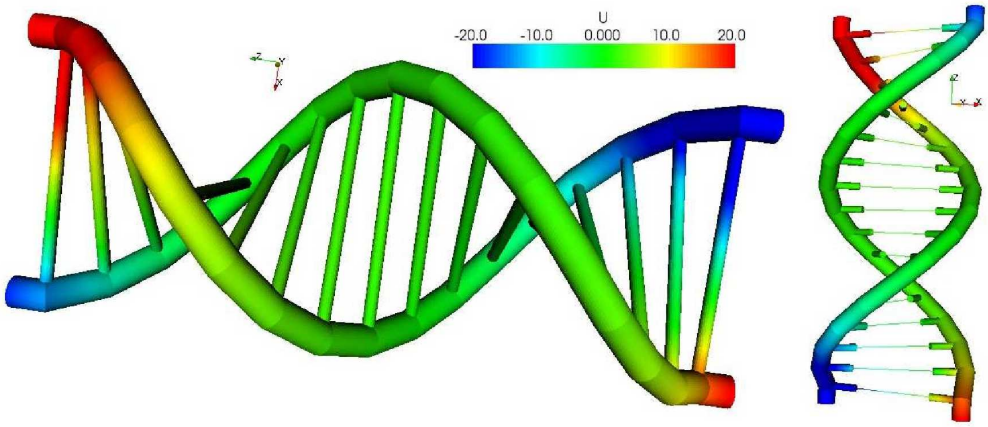

Results for the DNA-like mechanism
445x191mm (600 x 600 DPI)

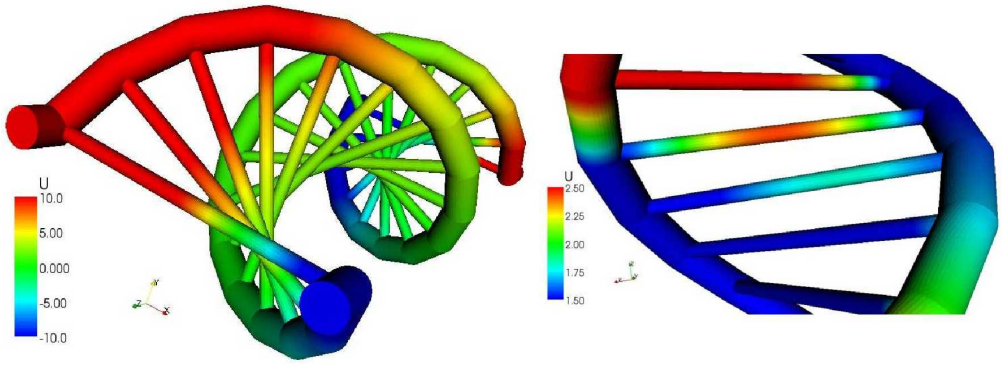

Details of the solution in the DNA-like mechanism
525x193mm (600 x 600 DPI)

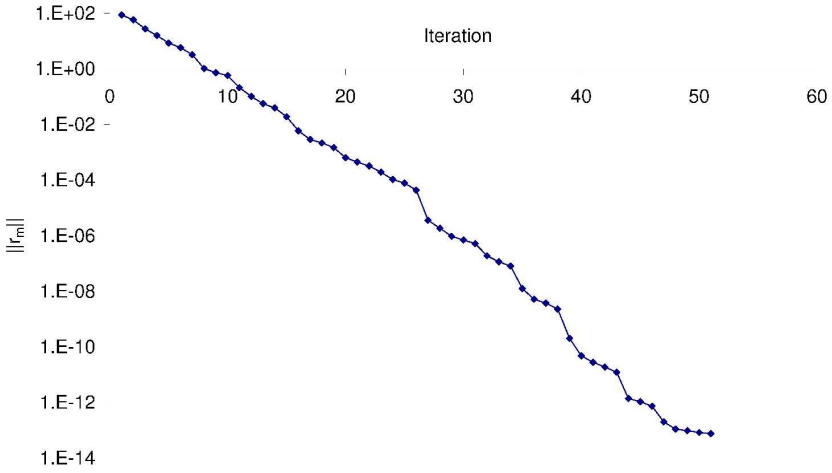

Convergence history of the residual $r_m=r(X_m)$ for the DNA-like mechanism
297x209mm (600 x 600 DPI)